RARE METALS
Vol. 30, Spec. Issue, Mar 2011, p. 16
DOI: 10.1007/s12598-011-0229-1

Design and modeling of electrolyte pumping power reduction in redox flow cells

Chih-Han Tian[a], Reiyu Chein[a], Kan-Lin Hsueh[b,c], Chun-Hsing Wu[c], and Fang-Hei Tsau[c]

[a] *Department of Mechanical Engineering, National Chung Hsing University, Taichung 402, Taiwan, China*

[b] *Department of Energy and Engineering, National United University, Miaoli 36003, Taiwan, China*

[c] *Green Energy & Environment Research Laboratories, Industrial Technology Research Institute, Hsinchu 31040, Taiwan, China*

Received 29 September 2010; received in revised form 29 December 2010; accepted 10 January 2011

Abstract

Because of flexible design, long life, and low-cost maintenance, redox flow cell has been recognized as one of the reliable energy storage techniques in remote power systems. In redox flow cells, electrolyte circulation through carbon felt is necessary in order to produce effective ion exchange during the charge and discharge operations. Pumping power required for electrolyte circulation could be significant, especially for multi-stack cell, due to low permeability of the porous carbon felt. Moreover, effective method for transporting bubbles formed inside the electrode is necessary for increasing the effective area of reaction of the electrodes. To further improve the overall performance of the redox flow cells, we proposed several novel designs of electrolyte inlet/outlet port and flow passage in carbon felt intending to reduce the electrolyte pumping power and to increase the effective area. Based on our numerical modeling, it is found that pumping power can be reduced by appropriate inlet/outlet port design and carbon felt with flow channel. The non-uniform flow pattern may cause the bubbles to be carried away from the electrodes effectively. The proposed designs can be applied not only for the single-stack cell but also applicable for the multiple-stacked cells.

Keywords: redox flow cell; electrolyte circulation; pumping power; porous carbon felt

1. Introduction

Renewable energy, such as wind turbine and photovoltaic, produces clean and sustainable energy. However, power produced from these devices is not a steady power. Electrical energy storage is needed to buffer the peak power on electrical grid. This becomes more critical in near future when the usage of renewable energy increases and smart grid and micro-gird implement. There are several available electricity storage technologies, namely hydro-pump, compressed air energy storage (CAES), and secondary batteries. Although the hydro-pump is the most matured and convenient storage for electrical energy, however, it is constrained by geometrical and environmental issues. Secondary battery, such as lead acid battery，is considered as the energy storage for stand alone photovoltaic system [1-2]. Due to limited life cycle, it can not be used for large scale energy storage. Lithium ion battery as well as nickel metal hydride battery has high energy storage density and efficiency. At present stage, they are not for large scale energy storage applications because of their safety and high cost. Redox flow battery is a promising energy storage technology due to low cost and long cycle life up to 13,000 cycles [3-6].

The principle of a redox flow battery involves coupled reversible electrochemical reactions. For the charging operation, reduction and oxidation reactions take place at the positive electrode and negative electrode, respectively. For the discharging operation, reversed reactions of the charging operation occur at the electrodes. An energy storage system of a redox flow battery contains two chemical storage tanks, two pumps, an electrolytic cell, and a converter. Extra electricity is converted into DC current via the converter and fed into the electrolytic cell. Electrolytes circulated by pumps between the electrolytic cell and storage tanks, are converted into high energy chemicals inside the cell during the charging from extra electricity. When electricity is needed, the high energy electrolytes are circulated between the cell and tanks and chemical energy is converted into DC power. The generated DC power from the electrolytic cell is converted into AC power via the converter [7-8].

There are several redox flow batteries under development. Vanadium redox battery (VRB) is the most mature energy storage technology among others [3]. It uses the same element (vanadium) in both positive and negative cell com-

Corresponding author: Reiyu Chein **E-mail:** rychein@dragon.nchu.edu.tw

partments to eliminate the cross contamination of reacting species. Many kW to MW VRB energy storage systems have been demonstrated worldwide. At present, the energy storage efficiency of VRB is around 80% [9-10]. Energy consumed by the circulation pump can be reduced to increase the storage efficiency. Most of the energy consumed by the circulation pump is to overcome the pressure gradient inside the electrolytic cell where the aqueous electrolyte is forcing flow through a porous carbon electrode. Configuration of the cell and design of the electrolyte flow pattern are the crucial issues for reducing the electrolyte pumping power consumption.

Most of the VRB researches focused on electrode characteristics for enhancing the battery efficiency and pay less attention to the flow channel and cell configuration designs for reducing the pumping power. Miyabayashi *et al*. [11] proposed a cell design with multiple inlets and outlets to reduce the pressure drop and to reach a uniform flow distribution pattern. Inoue *et al*. [12] proposed a porous electrode with internal hollow cavities. They pointed out that these cavities were able to reduce the pressure drop as the electrolyte flows across the entire electrode. Harper *et al*. [13] proposed a flow channel design on the bipolar plate similar to the flow channels used in proton exchange membrane fuel cell (PEMFC) to reduce the pressure drop and to obtain a uniformly distributed flow pattern. They further proposed an inter-digital channel design for the flow cell [14]. They claimed that the inter-digital channel design can enhance the cell performance without increasing the pressure drop significantly as the electrolyte flowing through the porous electrode. Moreover, the flow cell must satisfy the requirement that the contact area between the electrolyte and electrode is as large as possible. Failure of this requirement leads to low utilization of electrode and lower power density.

In this study, several novel designs on the electrolyte flow passage through the porous electrode are proposed. It is aimed to reduce the pressure drop further as the electrolyte flowing through the porous electrode. The pressure drop and flow pattern as the electrolyte flowing across the electrode are numerically predicted and compared.

2. Design model

The conventional design of a single stage VRB is composed by two equal-sized flow cells in rectangular shape. In one side of the VRB, porous electrode such as carbon felt is inserted in a rectangular-shaped cavity. Similar configuration is employed for the other side of the VRB. In between these two flow cells, ion exchange membrane such as Nafion is sandwiched. The entire system is assembled together by screw bolts around the edge of the battery. The electrolyte is introduced into the cell from the inlet port located at one of corners of the cell, circulated by a pump, and flows out of the cell from the corner opposite to the inlet port. The disadvantages of the conventional design are the flow non-uniformity which reduces the contact area between the electrolyte and electrode and high pressure drop which lowers the battery overall efficiency.

In this study, we propose six novel designs as shown in Fig. 1 in order to overcome the disadvantages in the conventional design. In these designs, flow channels are introduced for distributing the electrolyte as it flows into porous electrode and for collecting the electrolyte as it flows out of the porous electrode. All the designs shown in Fig. 1 have the same geometrical dimensions except the inlet/outlet ports and porous electrode designs. In our lab-scale VRB, the carbon felt electrode has the size of 100 mm × 100 mm × 3 mm. The flow channel for each design has the size of 100 mm × 10 mm × 3 mm. The features of the design shown in Fig. 1 are described below. In cell A shown in Fig. 1 (a), the electrolyte flows into and out of the cell with direction parallel to the flow channel. It is expected that such design may provide the convenience in the future multi-stack cell assembly. The cell B design shown in Fig. 1 (b) was originally proposed by Miyabayashi *et al*. [11]. It involves multiple inlet and outlet ports which are located perpendicularly to the flow channel. In the cell C design shown in Fig. 1 (c), large inlet and outlet port sizes are used with upcoming and outgoing flows perpendicular to the flow channel. For the designs of cells D, E, and F shown in Figs. 1 (d), (e), and (f), respectively, the inlet/outlet port designs are the same as that of cell C but with different porous electrode configurations. In these designs, channels with different patterns are cut in the porous electrode. One of the purposes of these channels is to further reduce the pressure drop as the flow over the porous electrode. The other purpose which may be important in the practical operation of VRB is that the cut channel may be used to carry the bubbles away from the electrode. The bubbles, resulted formed either from the dissolved gas in the electrolyte or water dissociation due to overcharge, are the undesired because they reduce the effective area of electrode and therefore need to be transported out of the electrodes. In cell D, each channel is dead-ended and has the length of 80 mm, width of 1 mm, and depth of 3 mm. For cell E, the channel design for the electrode is the same as that in cell D except that each channel is equipped with short branched channel. The length, width, and depth of the branched channel are as 5.7 mm, 1 mm, and 3 mm, respectively. In cell F, staggered arranged channels are cut inside the electrode. The length, width, and depth of each channel are 15, 1, 3 mm, respectively. Each channel was 5 mm apart.

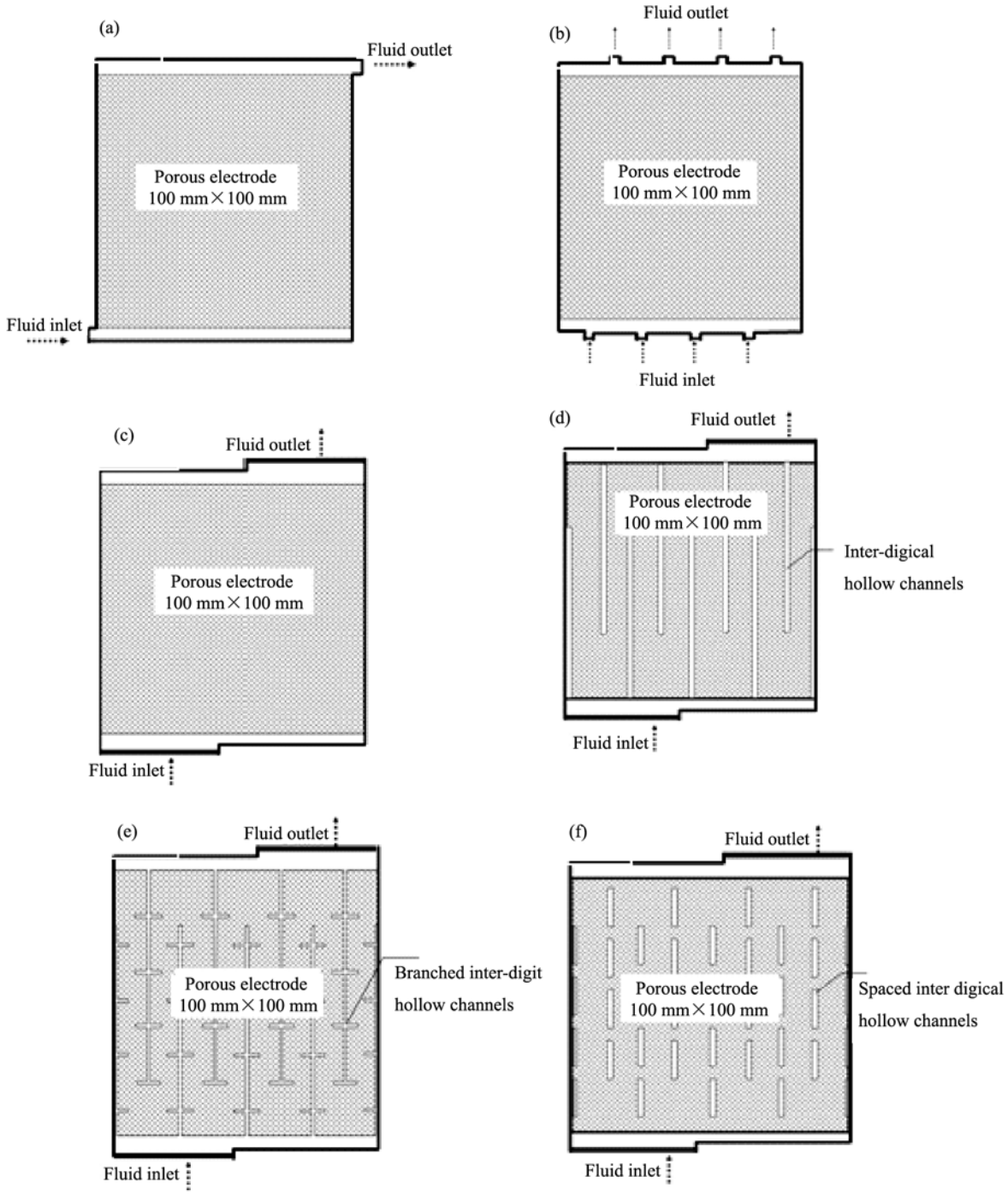

Fig. 1. Flow cell designs proposed in this study: (a) Cell A with single flow inlet/outlet, (b) Cell B with multiple flow inlet/outlet, (c) Cell C with wide single inlet/outlet, (d) Cell D with wide single inlet/outlet, inter-digit hollow channels in porous electrode, (e) Cell E with wide single inlet/outlet, branched inter-digit hollow channels in porous electrode, (f) Cell F with wide single inlet/outlet, staggered inter-digit hollow channels in porous electrode.

3. Theoretical and numerical models

The numerical simulation is carried out to evaluate the performance of each design described in Fig. 1. To avoid time-consuming three-dimensional computation, two-dimensional model was employed to investigate the flow patterns in the porous electrode [15]. We assume that the porous electrode can be treated as porous media having homogeneous porosity ε and permeability K. As shown in Fig. 1, there are two fluid domains involved in the computation: the clean-fluid domain in which no electrode appeared, and

the electrode domain where the porous electrode is placed. Under the steady-state condition, the governing equations for the fluid flow in these two domains can be written as [16],

Clear-fluid domain (flow channel and inlet/outlet ports):

$$\nabla \cdot \vec{V}_1 = 0 \tag{1}$$

$$\rho_f \vec{V}_1 \cdot \nabla \vec{V}_1 = -\nabla p_1 + \mu_1 \nabla^2 \vec{V}_1 \tag{2}$$

Porous electrode domain [17]:

$$\nabla \cdot \vec{V}_2 = 0 \tag{3}$$

$$\frac{\rho_f}{\varepsilon^2} \vec{V}_2 \cdot \nabla \vec{V}_2 = -\nabla p_2 + \frac{\mu_2}{\varepsilon} \nabla^2 \vec{V}_2 - \frac{\mu_2}{K} \vec{V}_2 - \frac{\rho_f C_F}{\sqrt{K}} \left|\vec{V}_2\right| \vec{V}_2 \tag{4}$$

In these equations, subscripts 1 and 2 refer to the clear fluid and the porous electrode subdomains, respectively. ρ_f, $\vec{V}$, μ, and ρ are the density, velocity vector, viscosity, and pressure of the electrolyte, respectively. Eq. (4) is known as the Brinkman-Darcy-Forchheimer model for the fluid flow in porous media with constant porosity. For flow in porous media, the fluid viscosity is usually assumed to be the same as that of a clear fluid, ie, $\mu_1 = \mu_2$. The porosity and permeability are two key factors that govern the fluid flow, heat transfer and mass transfer. In the VRB, carbon felt is usually employed as the electrode. The permeability and porosity would be important parameters in the VRB performance since they determine the mass transfer effectiveness as the electrolyte in contact with the electrode. In this study, various permeability and porosity values will be chosen and their effect on pressure drop will be compared. In Eq. (4), the Forchheimer drag coefficient C_F is given as [17],

$$C_F = 1.75 / (\sqrt{150} \varepsilon^{3/2}) \tag{5}$$

Boundary conditions must be specified to complete the mathematical model. Referring to Fig. 1, the boundary conditions are specified as follows,

(i) Inlet

Flow rate $Q = Q_{in}$, pressure $p = 0$ (6a)

(ii) Outlet

$$\frac{\partial \vec{V}_1}{\partial n} = 0 \text{ , } n\text{=direction normal to the outlet port.} \tag{6b}$$

(iii) Clear fluid-catalyst layer interface

$$\vec{V}_1 = \vec{V}_2, \quad p_1 = p_2, \mu_1 \frac{\partial \vec{V}_1}{\partial n} = \mu_2 \frac{\partial \vec{V}_2}{\partial n} \tag{6c}$$

(iv) Cell wall

$$\vec{V}_1 = \vec{V}_2 = 0 \tag{6d}$$

The boundary conditions shown in Eq. (6c) are known as the continuous conditions. At the interface, the fluid velocity, pressure, and their gradients must be equal at the interface between the clear-fluid and porous electrode.

All of the governing equations were solved simultaneously using the commercial finite element package COMSOL (version 3.3, http://www.femlab.com). The finite element calculations were performed using quadratic triangular elements. Because the accuracy of the numerical solutions strongly depends on the mesh size, a refined mesh is necessary in the region where the gradients of the dependent variable are pronounced. Finer meshes were used in this study in the regions around the clear fluid-porous electrode interface and near the cell wall to capture the subtle changes in fluid velocity. The solution independence on the mesh size was carefully studied before reporting the final results. The numerical results show that the solutions become mesh-independent when the element number exceeds approximately 16000. Hence, the results presented in this study were for 20000 to 30000 elements.

4. Results and discussion

Numerical calculations were carried out for each cell configuration at various electrode permeability (K), porosity (ε), and electrolyte volumetric flow rate (Q_{in}). Fig. 2 shows the typical result of streamlines for each design using $K = 1 \times 10^{-11}$ m^2, $\varepsilon = 0.7$, and $Q_{in} = 2$ L/h. The streamlines can be used to realize the flow pattern through the porous electrode. In general, uniform flow patterns can be observed for Cells A, B, and C and no local eddies or dead corners were found. Due to the cut channels in the electrode, the flow patterns of flow over the Cells D, E, and F are completely different from those of Cells A, B, and C. Instead of uniform flow over the electrodes, the electrolyte may penetrate through the cut channel with high velocity and then flow through the porous region of the electrode for the Cells D, E, and F. The large velocity difference between the flows in cut channel and in the porous electrode, may serve as the disturbance in the electrode that causing the bubbles to flow out of the electrode.

The predicted pressure drops across each cell as a function of inlet volumetric flow rate are shown in Figs. 3, 4, and 5 for $K = 1 \times 10^{-9}$ m^2, 1×10^{-10} m^2, and 1×10^{-11} m^2, respectively. All the pressure drops are seen to vary linearly with the electrolyte flow rate. As expected, the pressure drop increases with the decrease in porous electrode permeability. Based on the results shown in Figs. 3, 4, and 5, the order of magnitude of the pressure drop among the six designs is C > A > B > F > D > E under a given flow rate. Another important conclusion from the pressure drop results is that the pressure drop across the porous electrode can be reduced by the introduction of channel in the porous electrode.

Although the pressure drop can be reduced by using the channeled porous electrode, electrode active area is reduced. The reduction of electrode active area causes the reduction

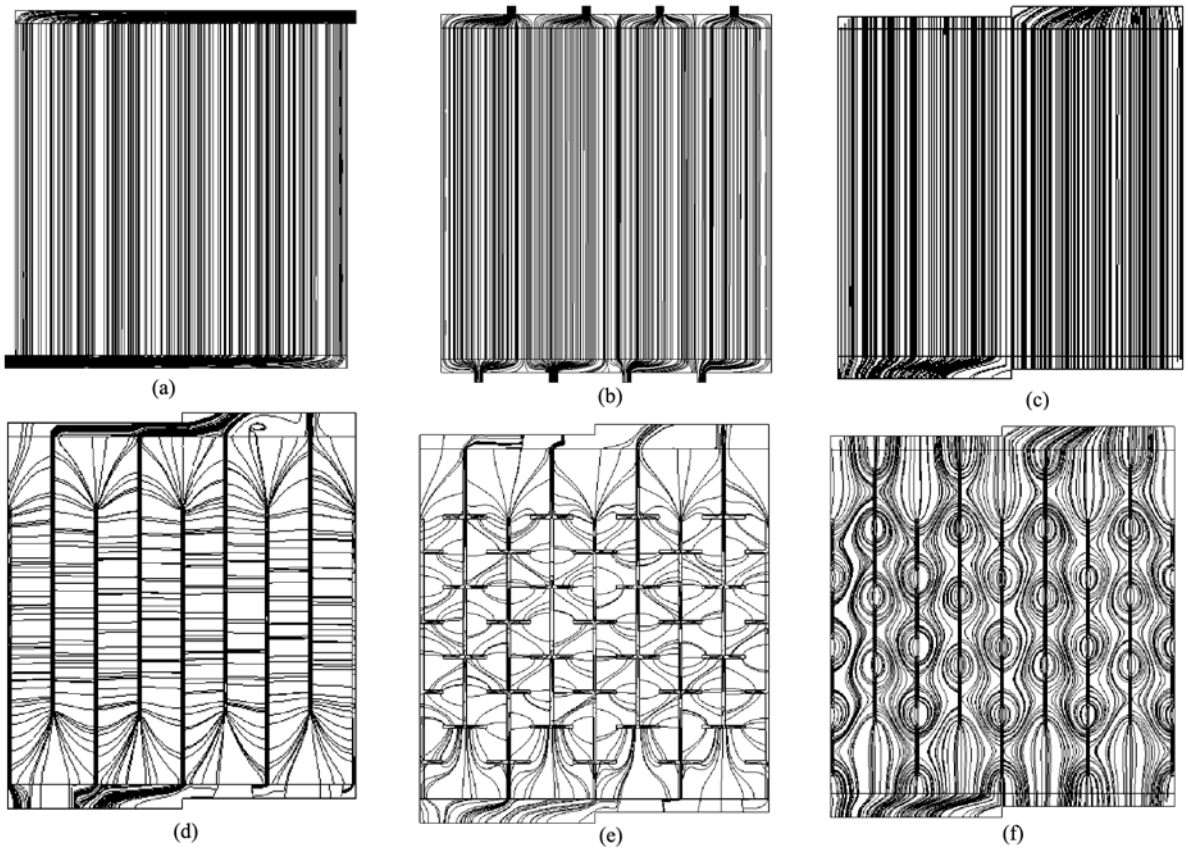

Fig. 2. Streamlines inside the cells $K = 1 \times 10^{-11}$ m^2, $\varepsilon = 0.7$, and $Q_{in} = 2$ L/h: (a) cell A, (b) cell B, (c) cell C, (d) cell D, (e) cell E, (f) cell F.

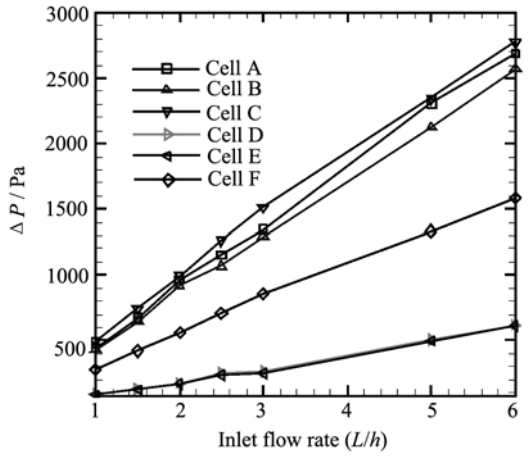

Fig. 3. Pressure drop across the cell as function of electrolyte flow rate. $K = 1 \times 10^{-9}$ m^2, and $\varepsilon = 0.7$.

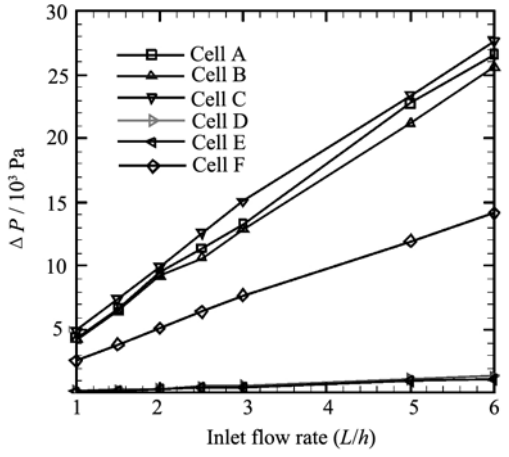

Fig. 4. Pressure drop across the cell as function of electrolyte flow rate. $K = 1 \times 10^{-10}$ m^2, and $\varepsilon = 0.7$.

of output current at a given cell voltage. A simplified model is described below to evaluate the net power output of each cell design shown in Fig. 1. The net power output from the cell (P_{net}) is equal to the power output from the cell (P_{cell}) minus the pumping power (P_{pump}) required for circulating the fluid, ie,

$$P_{net} = P_{cell} - 2P_{pump} \tag{7}$$

where P_{cell} is the product of cell voltage (E), current density (i), and electrode active area (A).

$$P_{cell} = EiA \tag{8}$$

For typical VRB, the current density and cell voltage are taken as 0.03 A/cm^2 and 1.5 Volt, respectively. The power consumed by the pumps is given as

$$P_{pum} = Q_{in}\Delta p \tag{9}$$

where ΔP is the pressure drop. Table 1 shows the performances of the cell designs for flow rate of 5 L/h based on Eqs. (7-9). As indicated in Table 1, cell D has the best net power output among the designs shown in Fig. 1.

Table 1. Net power output of VRB with various flow cell and electrode designs (Q_{in} = 5 L/h, $K = 1 \times 10^{-11}$ m^2)

Cell	A	B	C	D	E	F
Output power from cell, P_{cell} (W)	4.5	4.5	4.5	4.176	4.028	4.257
Power consumed by pump, P_{pump} (W)	0.45	0.42	0.47	0.01	0.007	0.234
Net power output, P_{net} (W)	3.6	3.66	3.56	4.156	4.014	3.789

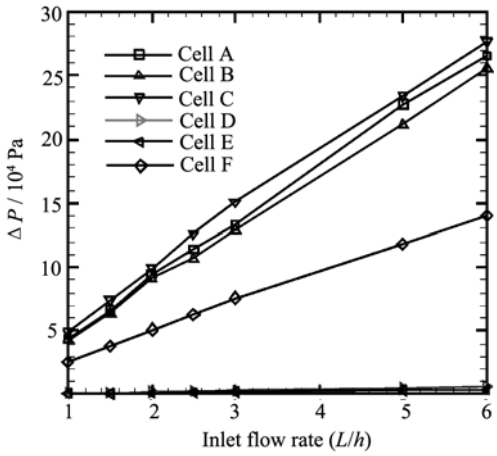

Fig. 5. Pressure drop across the cell as function of electrolyte flow rate. $K = 1 \times 10^{-11}$ m^2, and $\varepsilon = 0.7$.

5. Conclusion

In this study, novel designs on reducing the pressure drop across the porous electrodes in VRB were proposed and numerically studied. For the lab-scale single electrode size, we found that the pressure drop can be reduced by the introduction of channels in the flow cell and electrode designs. Instead of directly injecting the electrolyte as done in conventional design the introduction of flow distribution and collection channels outside the porous electrode can produce better flow uniformity through the electrode. By the introduction of channels inside the porous electrode, the pressure drop can be reduced and does not produce significant net power output loss.

References

[1] Fabjan C., Garche J., Harrer B., Jörissen L., Kolbeck C., Philippi F., Tomazic G., and Wagner F., The vanadium redox-battery: an efficient storage unit for photovoltaic systems, *Electrochimica Acta,* 2001, **47**: 825.

[2] Joerissen L., Garche J., Fabjan C., and Tomazic G., Possible use of vanadium redox-flow batteries for energy storage in small grids and stand-alone photovoltaic systems, *J. Power Sources*, 2004, **127**: 98.

[3] Ponce de Leon C., Frıas-Ferrer A., Gonzalez-Garcıa J., Szanto D.A., and Walsh F.C., Redox flow cells for energy conversion, *J. Power Sources,* 2006, **160**: 716.

[4] Sum E., Rychcik M., and Skyllas-Kazacos M., Investigation of the V(V)/V(IV) system for use in the positive half-cell of a redox battery, *J. Power Sources,* 1985, **16**: 85.

[5] Bartolozzi M., Development of redox flow batteries. A historical bibliography, *J. Power Sources,* 1989, **27**: 219.

[6] Skyllas-Kazacos M., and Robins R., *All Vanadium Redox Battery,* US Patent, 849, 094, 1986.

[7] Tokuda N., Kanno T., Hara T., Shigematsu T., Tsutsui Y., Ikeuchi A., Itou T., and Kumamoto T., Development of a redox flow battery system, *SEI Technical Review,* 2000, **50**: 88.

[8] Li M., and Hikhara T., A coupled dynamical model of redox flow battery based on chemical reaction, fluid flow, and electrical circuit, *Ieice Trans. Fundamentals*, 2008, E91-A(7): 1741.

[9] Shah A.A., Watt-Smith M.J., and Walsh F.C., A dynamic performance model for redox-flow batteries involving soluble species, *Electrochimica Acta,* 2008, **53**: 8087.

[10] Jia C., Liu J., and Yan C., A significantly improved membrane for vanadium redox flow battery, *J. Power Sources,* 2010, **195**: 4380.

[11] Miyabayashi M., Sato K., Tayama T., Kageyama Y., and Oyama H., *Redox Flow Type Battery,* US Patent 5 851 694, 1998.

[12] Inoue M., and Kobayashi M., *Electrode Material for Flow Through Type Electrolytic Cell, Wherein the Electrode Comprises Carbonaceous Material Having at Least One Groove*, US Patent, 5 648 184, 1997.

[13] Harper M.A.M., *Electrochemical Battery Incorporating Internal Manifolds,* US Patent, 7 682 728, 2010.

[14] Harper M.A.M., *Electrochemical Battery Incorporating Internal Manifolds,* US Patent, 7 687 193, 2010.

[15] Sun C., Chen J., Zhang H., Han X., and Luo Q., Investigations on transfer of water and vanadium ions across Nafion membrane in an operating vanadium redox flow battery, *J. Power Sources,* 2010, **195**: 890.

[16] Bird B., Stewart W., and Lightfoot E., *Transport Phenomena*, 2nd ed., John Wiley and Sons, NY, USA, 2002.

[17] Nield D.A., and Bejan A., *Convection in Porous Media*. Springer Science-Business Media, New York, USA, 2006.